VORTICITY, STRAIN AND LARGE SCALE STATISTICS AS A FUNCTION OF THE SHEAR PARAMETER AND REYNOLDS NUMBER IN HOMOGENEOUS TURBULENT SHEAR FLOW

Juan C. Isaza
Sibley School of Mechanical & Aerospace Engineering
Cornell University
Ithaca, NY, 14850, US
ji27@cornell.edu

Lance R. Collins
Sibley School of Mechanical & Aerospace Engineering
Cornell University
Ithaca, NY, 14850, US
LC246@cornell.edu

ABSTRACT

The asymptotic behavior of large- and small-scale velocity statistics in an homogeneous turbulent shear flow is examined using direct numerical simulations of the incompressible Navier-Stokes equations on a 512^3 grid. We used a novel pseudo-spectral algorithm (Brucker et al. 2007) that allows us to set the initial value of the shear parameter in the range 3–30. We have found that large-scale quantities such as the ratio of kinetic energy production over dissipation, and the nondimensional shear parameter reach a self-similar state that depends sensitively on the initial value of the shear parameter. Additionally, we show that the probability density function (PDF) of the vorticity vector and the rate-of-strain tensor approach a Gaussian distribution with increasing initial shear parameter. On the other hand, the tails of the PDFs of the velocity derivatives become more stretched with increasing Reynolds number at fixed shear parameter. We use Viscous Rapid Distortion Theory to explain some of these trends.

INTRODUCTION

Homogeneous shear flow is considered to be one of the building blocks of turbulence. It is the next step up in complexity from isotropic turbulence. This flow has the main features of wall-bounded flows, i.e., Reynolds stress, turbulence production, hairpin vortices, without introducing the complexities of fully inhomogenous turbulence. Consequently, this flow has been widely investigated in experiments and direct numerical simulations.

Experimental work suggests the turbulent kinetic energy and the integral length scale grow in time, approaching an asymptotic state at long times (Harris *et al*, 1977; Tavoularis and Corrsin, 1981; Rohr *et al*, 1988; Tavoularis and Karnik, 1989, De Souza *et al*, 1995). Direct numerical simulations (DNS) of homogeneous turbulent shear flow support these claims (Lee *et al*, 1990; Shih *et al*, 2000; Yu and Girimaji, 2005; Jacobitz *et al*, 1997; Jacobitz and Sarkar, 1999; Kida and Tanaka, 1992).

Homogeneous shear flow is characterized by the initial values of two parameters: the Reynolds number, R_λ, here defined in terms of the Taylor microscale;[1] and the shear paramater, S_0^*.[2] Whether the asymptotic state of the flow is a function of the initial value of those parameters remains a controversy. Jacobitz *et al*, (1997) and Shih *et al*, (2000) suggest that it is, whereas the Yu and Girimaji (2005) remark that S_0^* will only weakly affect the asymptotic statistics.

In this report, we address this controversy through a series of 512^3 DNS using a new pseudo-spectral algorithm for purely homogeneous turbulent shear flow that circumvents the shortcomings of previous numerical schemes, allowing us to vary the initial value of the shear parameter over the range 3–30. We study the influence of the shear parameter on large-scale and small-scale statistics. The results for the high shear cases are compared with the predictions of Viscous Rapid Distortion Theory (VRDT).

PROBLEM DEFINITION

Governing Equations

We are interested in the flow of an incompressible fluid in a periodic box of length 2π in each direction. The governing equations for the fluid, in rotational form, are

$$\frac{\partial u_i}{\partial x_i} = 0 \ , \tag{1}$$

$$\frac{\partial u_i}{\partial t} + \epsilon_{ijk}\ \omega_j\ u_k = -\ \frac{\partial \left(p/\rho + \frac{1}{2}u^2\right)}{\partial x_i} + \nu\ \frac{\partial^2 u_i}{\partial x_j \partial x_j} \ , \tag{2}$$

where u_i is the velocity vector, $u \equiv \sqrt{u_i u_i}$ is the magnitude of the velocity vector, ρ is the fluid density, ν is the kinematic viscosity, ϵ_{ijk} is the alternating unit symbol, $\omega_i = \epsilon_{ijk}\ \frac{\partial u_k}{\partial x_j}$ is the vorticity, and p is the pressure.

Introducing the Reynolds decomposition, $u_i = U_i + u_i'$, $\omega_i = \Omega_i + \omega_i'$ and $p = P + p'$, where capital letters represent mean quantities and prime letters fluctuating quantities. For shear flow we take $U_i = (\mathcal{S}x_2, 0, 0)$, $\quad \Omega_i = (0, 0, -\mathcal{S})$ where

[1] $R_\lambda \equiv q_0^2\sqrt{15/\nu\epsilon_0}$, where $q_0^2/2$ is the initial turbulent kinetic energy, ν is the kinematic viscosity, and ϵ_0 is the initial dissipation rate.

[2] $S_0^* \equiv \mathcal{S}q_0^2/2\epsilon_0$, where $\mathcal{S}$ is the spatially and temporally uniform mean shear imposed on the flow.

$\mathcal{S}$ is the spatially uniform mean shear rate. Invoking homogeneity and combining and simplifying the terms that involve the mean flow, the final form of the equation for the fluctuating velocity is

$$\frac{\partial u_i'}{\partial t} + \mathcal{S}x_2\frac{\partial u_i'}{\partial x_1} + \mathcal{S}\delta_{i1}u_2' + \epsilon_{ijk}\omega_j'u_k' = -\frac{\partial p^*}{\partial x_i} + \nu\frac{\partial^2 u_i'}{\partial x_j \partial x_j}\ , \tag{3}$$

where $p^* \equiv p'/\rho + \frac{1}{2}u'^2$ is the modified pressure.

Numerical Algorithm

The boundary condition for Eq. (3) in the x_2 direction is not periodic in the laboratory frame of reference due to the presence of the uniform shear. Figure (1) shows a schematic of the boundary condition in two dimensions. The dashed lines show the deforming frame of reference in which the flow is periodic. The solid lines indicate the orthogonal frame of reference. Forward and reverse spectral transforms for a generic variable ϕ in the orthogonal frame of reference are defined as follows (Brucker et al. 2007)

$$\phi(\mathbf{x},t) = \frac{1}{N^3}\sum_{\mathbf{k}}\hat{\phi}(\mathbf{k},t)\exp\left[I\left(k_i x_i - \mathcal{S}tk_1x_2\right)\right]\ , \tag{4}$$

$$\hat{\phi}(\mathbf{k},t) = \sum_{\mathbf{x}}\phi(\mathbf{x},t)\exp\left[-I\left(k_i x_i - \mathcal{S}tk_1x_2\right)\right]\ , \tag{5}$$

where $I \equiv \sqrt{-1}$. The cross term in the exponential, $\mathcal{S}tk_1x_2$, arises due to the shear-periodic boundary condition. As a consequence of this term, it is not possible to calculate the forward and reverse transforms using a standard 3D FFT.

Rogallo (1981) resolved this issue by transforming Eq. (3) into a coordinate system that moves with the mean flow (dashed line in Fig. 1). In this moving frame of reference, the spectral transform reduces to the conventional 3D Fourier transform, allowing the use of a standard 3D FFT. However, mean convection causes a distortion of the mesh in physical space, leading to a growth in aliasing errors that are incurred during the evaluation of the nonlinear terms on the deformed mesh. To relieve this problem, Rogallo introduced a remeshing step. Remeshing with dealiasing leads to a sudden loss in both the turbulent kinetic energy and turbulent energy dissipation rate. For higher shear rates, this loss can be significant (20–40%; Lee *et al*, 1990).

We developed an alternative algorithm that works directly with Eqs. (4) and (5) in the orthogonal (laboratory) frame of reference. The challenge was to accomplish the 3D transform, with the phase shift, in $O(N^3 \ln N)$ operations, where N is the number of grid points in each direction. This was accomplished by decomposing the three-dimensional transform into a sum of products of one- and two-dimensional transforms (i.e., pencils and planes). The performance and validation of this new algorithm with experiments and the Rogallo algorithm is discussed extensively in Brucker *et al* (2007).

Initial Conditions

The initial velocity field was generated using a random phase algorithm with a prescribed initial energy spectrum given by

$$E(k) = C_\kappa \epsilon_0^{2/3}\kappa_0^{-5/3}\begin{cases}(k/\kappa_0)^2 & k < \kappa_0\\ (k/\kappa_0)^{-5/3} & \kappa_0 \leqslant k \leqslant \kappa_\eta\\ 0 & k > \kappa_\eta\end{cases}\ , \tag{6}$$

where $C_\kappa \approx 1.5$ is the Kolmogorov constant, ϵ_0 is the initial energy dissipation rate, κ_0 is the wavenumber where the peak in the energy spectrum occurs, and κ_η is the maximum energy-containing wavenumber, defined to be consistent with ϵ_0 as

$$\frac{\kappa_\eta}{\kappa_0} \equiv \left[\frac{2\epsilon^{1/3}}{3\nu C_\kappa \kappa_0^{4/3}} + \frac{11}{15}\right]^{3/4}\ . \tag{7}$$

Note that in the study of the small-scale statistics, we first allowed the initial velocity to decay by performing an isotropic DNS without shear until the velocity derivative skewness, $\left\langle (\frac{\partial u_1}{\partial x_1})^3\right\rangle / \left\langle (\frac{\partial u_1}{\partial x_1})^2\right\rangle^{3/2}$, reached a value of -0.4. This allowed the small scales to evolve to a more natural state before applying the uniform shear. This initial velocity field also was used in all of the comparisons with VRDT.

Because the initial shape of the energy spectrum is fixed by Eq. (6), the turbulent shear flow is parameterized by: the initial Reynolds number based on the Taylor microscale, R_λ; and the initial value of the shear parameter, S_0^*. A goal of this study is to understand the dependence of the self-similar statistics on these two parameters.

Computational Resolution

In homogeneous turbulent shear flow, the large scales grow and the small scales decrease with time. We choose the peak wavenumber, κ_0, to control the initial integral length scale so that it has room to grow within the box over the duration of the DNS. Criteria must be developed for the point in time that the simulation should be stopped due to loss of resolution. Ideally, each run will fail at the large and small scales simultaneously. We try to choose the location of the peak in the initial energy spectrum such that this happens. Experimentally it has been found that the longitudinal length scale, $L_{11,1}$,[3] grows monotonously with time (Harris *et al*, 1977; Tavoularis and Corrsin, 1981; Rohr *et al*, 1988; Tavoularis and Karnik, 1989, De Souza *et al*, 1995). Consequently, we stopped our calculations when $dL_{11,1}/dt \leqslant 0$.

Resolution of the small scales requires that $k_{\max}\eta \geqslant 1$, where $k_{\max} \equiv \sqrt{2}N/3$ is the maximum wavenumber and $\eta \equiv \left(\nu^3/\epsilon\right)^{1/4}$ is the Kolmogorov length scale. Simulations were discontinued when $k_{\max}\eta$ dropped below unity.

RESULTS

Influence of the Shear Parameter on Large-Scale Statistics

As noted in the introduction, there is some question concerning the sensitivity of the asymptotic turbulence statistics in turbulent shear flow to the initial shear parameter, S_0^*. If the flow were insensitive, we would expect the evolution of $S^*(\mathcal{S}t)$ at long times (large $\mathcal{S}t$), would be independent of S_0^*. Figure 2 shows the time evolution of S^* for various initial conditions. Notice that each of the curves reaches an apparent asymptotic value that depends sensitively upon the initial value. It is important to note that most of the earlier experimental and computational studies of homogeneous turbulent shear flow have been restricted to values of the shear parameter below 10, as can be seen in Fig. 3. Exceptions include the experiments of De Souza *et al*, (1995) that reached an experimental value of 21 and the simulations of Lee *et al*, (1990) and Jacobitz and Sarkar, (1999) that reached of 30. We have seen in our DNS that when

[3] $L_{11,1} = \int_0^\infty f_{11}(r)dr$,
where $f_{11}(r) = \left\langle u_1'(x_1)u_1'(x_1+r)\right\rangle / \left\langle u_1'^2\right\rangle^{1/2}$.

S_0^* is below 10, the asymptotic statistics are insensitive to it. It is only for $S_0^* > 10$ that the dependence on S_0^* is observed. This may, in part, explain why the influence of this parameter has been so controversial.

If we define the anisotropic Reynolds stress coefficient as $b_{12} \equiv -\langle u_1' u_2' \rangle / q^2$, we expect this quantity to approach a steady value in the asymptotic regime. Figure 4 shows the time evolution of $b_{12}(\mathcal{S}t)$; once again, we observe the asymptote is a function of the initial shear parameter. The anisotropy of the flow decreases as the shear parameter increases. A similar trend was reported by Yu and Girimaji (2005) and Jacobitz and Sarkar, (1999).

If we define the production of turbulent kinetic energy as, $\mathcal{P} \equiv -\mathcal{S}\langle u_1' u_2' \rangle$, then we see that the ratio of kinetic energy production to dissipation can be written as $\mathcal{P}/\epsilon = 4 b_{12} S^*$, hence the asymptotic behavior of $\mathcal{P}/\epsilon$ is controlled by the asymptotic behaviors of $b_{12}(\mathcal{S}t)$ and $S^*(\mathcal{S}t)$. Figure 5 shows the behavior of $\mathcal{P}/\epsilon$ for three initial values of S_0^*. We observe the long term asymptotes are again sensitive to S_0^*.

Influence of the Shear Parameter on Small-Scale Statistics

It is known that the probability density function (PDF) of the velocity derivatives in turbulence deviates from the Gaussian distribution (Shen and Warhaft, 2000). Figures 6 and 7 show the time evolution of the PDFs of $s_{11} = \partial u_1/\partial x_1$ and $s_{33} = \partial u_3/\partial x_3$ over the time frame $4 \leqslant \mathcal{S}t \leqslant 10$ for the highest shear case ($S_0^* = 26.9$). The solid curve in the plots represents a Gaussian distribution with zero mean and unit variance. Notice that the PDFs deviate from the Gaussian curve in different ways. The s_{11} component is negatively skewed, as would be expected in isotropic turbulence, however by an amount that increases with time. The PDF of s_{33}, in contrast, is symmetric, with tails that progressively stretch with time. This may be correlated to the simultaneous growth in R_λ with time (from 30 to 70).

Figures 8 and 9 show the equivalent PDFs of vorticity components ω_1 and ω_3 over the same time interval $4 \leqslant \mathcal{S}t \leqslant 10$. As with the strain, they each deviate from the Gaussian distribution differently. The PDF of ω_1 (and ω_2 not shown) is symmetric with stretched exponential tails while the PDF of ω_3 is strongly skewed. This asymmetry is due to the presence of the mean shear that enhances vorticity that is aligned with the mean vorticity. The PDFs become more stretched as time progresses as a result of the increasing R_λ (30–70). On the other hand, for a fixed R_λ and increasing S^* the PDF of the vorticity approaches a Gaussian distribution, as can be seen in Fig. 10.

Viscous Rapid Distortion Theory

As suggested by Hunt and Carruthers (1990), Lee *et al* (1990), Rogers (1991) and others, when the mean deformation rate is large compared to the turbulence time-scales, the governing equations can be linearized by neglecting turbulence–turbulence interactions. In this "rapid" limit, the spectral transform of Eq. (3) has an analytical solution

$$\hat{\mathbf{u}}'(\mathbf{k}, t) = \exp(-\Gamma)\, \mathbf{A} \cdot \hat{\mathbf{u}}'(\mathbf{k}_0, 0) \ ,$$

where

$$\mathbf{A} = \begin{bmatrix} 1 & \frac{k_0^2}{k_{13}^2}\left(-\frac{k_3^2}{k_0^2}P + \frac{k_1^2}{k_0^2}Q\right) & 0 \\ 0 & \frac{k_0^2}{k^2} & 0 \\ 0 & \frac{k_1 k_3}{k_{13}^2}(P+Q) & 1 \end{bmatrix} \tag{8}$$

$$k_0^2 = \left(k_1^2 + k_2^2 + k_3^2\right) \tag{9}$$

$$k^2 = \left(k_0^2 - 2k_1 k_2 \mathcal{S}t + (k_1 \mathcal{S}t)^2\right) \tag{10}$$

$$k_{13}^2 = \left(k_1^2 + k_3^2\right) \tag{11}$$

$$\Gamma = \nu t \left[k_0^2 - k_1 k_2 \mathcal{S}t + \frac{(k_1 \mathcal{S}t)^2}{3}\right] \tag{12}$$

$$Q = \frac{\mathcal{S}t\left(k_0^2 - 2k_2^2 + k_1 k_2 \mathcal{S}t\right)}{k^2} \tag{13}$$

$$\alpha = \frac{k_2}{\sqrt{k_1^2 + k_3^2}} \tag{14}$$

$$\beta = \frac{k_2 - k_1 \mathcal{S}t}{\sqrt{k_1^2 + k_3^2}} \tag{15}$$

$$P = \frac{k_0^2}{k_1\sqrt{k_1^2 + k_3^2}}\left(\arctan\alpha - \arctan\beta\right) \tag{16}$$

From the equation for $\hat{\mathbf{u}}'(\mathbf{k}, t)$, we can construct the 3D velocity spectrum tensor

$$\Phi_{ij} = \exp(-2\Gamma)\, A_{ip} A_{jq} \Phi_{pq}^0 \tag{17}$$

where the matrix $\mathbf{A}$ and Γ are defined above. Φ_{pq}^0 is the initial 3D velocity spectrum that is assumed to be isotropic (Townsend, 1979)

$$\Phi_{ij}^0 = \frac{E(k)}{4\pi k^2}\left(\delta_{ij} - \frac{k_i k_j}{k^2}\right) \tag{18}$$

where k_i is the wave vector and k its magnitude. $E(k)$ is the initial energy spectrum that was obtained by the initialization procedure describe earlier.

Once the spectrum is known, it is possible to integrate the equation over spectral space to evaluate single-point turbulence statistics like the Reynolds stress tensor. Since we include viscosity in our formulation, we can calculate the energy dissipation rate and use it to compute the time evolution of the shear parameter and the ratio of turbulence production over dissipation. For short times (i.e., in the limit $\mathcal{S}t \to 0$), we follow the procedure of Rogers (1991), Townsend (1976), Livescu (2004), and others, to obtain

$$\frac{\mathcal{P}}{\epsilon}(\mathcal{S}t) = \frac{2}{15} S_0^* \mathcal{S}t - \frac{1}{10}(\mathcal{S}t)^2 + C_1 (\mathcal{S}t)^2 + \cdots \ , \tag{19}$$

$$\frac{S^*(\mathcal{S}t)}{S_0^*} = 1 + \frac{1}{S_0^*}\mathcal{S}t - \frac{11}{210}(\mathcal{S}t)^2 + \frac{2}{(S_0^*)^2}(\mathcal{S}t)^2 + \cdots \ , \tag{20}$$

where C_1 is a coefficient that depends on the shape of the initial energy spectrum. The expansion reveals an explicit dependence of $\mathcal{P}/\epsilon$ and S^* on S_0^*. Figures 11 and 12 compare the numerical predictions of VRDT with the DNS. As expected, the theory is accurate for short times ($\mathcal{S}t < 5$). VRDT eventually fails to predict the dissipation rate accurately. Figure 13 shows the spectra at $\mathcal{S}t = 2$ and $\mathcal{S}t = 8$, demonstrating that the linear theory underpredicts the high wavenumber range of the turbulent kinetic energy spectrum. Consequently, VRDT cannot offer insight into the role of the shear parameter at long times. There are two possible origins of this failure. First, the exponential term in the VRDT equation will cause the kinetic energy to decay to zero at long times. Second, the equation neglects turbulence-turbulence interactions that are responsible for (among other things) the turbulent energy cascade from low to high wavenumbers. It seems plausible that the latter issue is causing the more significant error at long times because as time progresses the energy at high wavenumbers is not replenished by the nonlinear interactions that are neglected by VRDT.

This suggests that no matter how large the value of S_0^*, the nonlinear terms eventually become relevant as $\mathcal{S}t \to \infty$.

CONCLUSIONS

A new spectral code was used to study the effect of the shear parameter on the time evolution of large- and small-scale statistics in an homogeneous turbulent shear flow. The new code allows us to vary the the initial values of the shear parameter, S_0^*, over a relatively wide range, 3–30. Our findings suggest that the asymptotic behavior of large-scale statistics such as $\mathcal{P}/\epsilon$, b_{12} and S^* are sensitive to S_0^* over the limited range of R_λ considered. We showed that the PDF of components of the vorticity vector and the rate-of-strain tensor approach a Gaussian distribution with increasing S_0^*. In contrast, the tails of the PDFs become more stretched with increasing Reynolds number at fixed S_0^*, consistent with experiments. VRDT predicts the dependence of $\mathcal{P}/\epsilon$ and S^* on S_0^* at short times; however, VRDT cannot predict the high wavenumber part of the energy spectrum at long times. The result suggests that nonlinear interactions eventually become important in the dynamics of turbulent shear flows with arbitrarily large S_0^*.

ACKNOWLEDGMENTS

This work was financially supported by the National Science Foundation under grants PHY-0216406 and PHY-0554675. JCI was supported by a fellowship from the Fulbright Commission and EAFIT University in Colombia.

REFERENCES

Brucker, K. A., Isaza J. C., Vaithianathan T. and Collins L. R., 2007, "Efficient Algorithm for Simulating Homogeneous Turbulent Shear Flow without Remeshing," *J. Comput. Phys.*, in press.

De Souza F. A., Nguyen V. D. and Tavoularis S., 1995, "The Structure of Highly Sheared Turbulence," *J. Fluid Mech.*, Vol. 303, pp. 155-167.

Harris V.G., Graham J. A. H. and Corrsin S., 1977, "Further Experiments in Nearly Homogeneous Turbulent Shear Flows," *J. Fluid Mech.*, Vol. 81, pp. 657-687.

Hunt J. C. R. and Carruthers D. J., 1990, "Rapid Distortion Theory and the 'Problems' of Turbulence," *J. Fluid Mech.*, Vol. 212, pp. 497-532.

Jacobitz F. G., Sarkar S. and Van Atta C. W., 1997, "Direct Numerical Simulations of the Turbulence Evolution in a Uniformly Sheared and Stably Stratified Flow," *J. Fluid Mech.*, Vol. 342, pp. 231-261.

Jacobitz F. G. and Sarkar S., 1999, "On the Shear Number Effect in Stratified Shear Flow," *Theoret. Comput. Fluid Dynamics*, Vol. 13, pp. 171-188.

Kida S. and Tanaka M., 1992, "Reynold Stress and Vortical Structure in a Uniformly Sheared Turbulence," *J. Phy. Soc. Japan*, Vol 61, pp. 4400-4417.

Lee M. J., Kim J. and Moin P., 1990, "Structure of Turbulence at High Shear Rate," *J. Fluid Mech.*, Vol. 216, pp. 561-583.

Livescu D. and Madnia C. K., 2004, "Small Scale Structure of Homogeneous Turbulent Shear Flow," *Phys. Fluids*, Vol. 16, pp. 2864-2876.

Shih L., Koseff J. R., Ferziger J. H. and Rehmann C. R., 2000, "Scaling and Parameterization of Stratified Homogeneous Turbulent Shear Flow," *J. Fluid Mech.*, Vol. 412, pp. 1-20.

Tavoularis S. and Corrsin S., 1981, "Experiments in Nearly Homogeneous Turbulent Shear Flows with a Mean Temperature Gradient. Part 1," *J. Fluid Mech.*, Vol. 104, pp. 311-347.

Tavoularis S. and Karnik U., 1989, "Further Experiments on the Evolution of Turbulent Stresses and Scales in Uniformly Sheared Turbulence," *J. Fluid Mech.*, Vol. 204, pp. 457-478.

Townsend A. A., 1976, "The Structure of Turbulent Shear Flow," *Cambridge University Press*, 2^{nd} ed.

Rogallo R. S., 1981, "Numerical Experiments in Homogeneous Turbulence," *NASA Tech. Memo.*, 81315.

Rogers M. M., 1991, "The Structure of a Passive Scalar Field with a Uniform Mean Gradient in a Rapidly Sheared Homogeneous Turbulent Flow," *Phys. Fluids A*, Vol. 3 (1), pp. 144-154.

Rogers M. M., Moin P. and Reynolds W. C., 1986, "The Structure and Modeling of the Hydrodynamic and Passive Fields in Homogeneous Turbulent Shear Flow," *Report No.* TF-25.

Rohr J. J., Itsweire E.C., Helland K. N. and Van Atta C. W., 1988, "An Investigation of the Growth of Turbulence in a Uniform-Mean-Shear Flow," *J. Fluid Mech.*, Vol. 187, pp. 1-33.

Schumacher J., Sreenivasan K. R. and Yeung P. K., 2003, "Derivative Moments in Turbulent Shear Flows," *Phys. Fluids*, Vol. 15, pp. 84-90.

Schumacher J., 2004, "Relation Between Shear Parameter and Reynolds Number in Statistically Stationary Turbulent Shear Flows," *Phys. Fluids*, Vol. 16, pp. 3094-3102.

Shen X. and Warhaft Z., 2000, "The Anisotropy of the Small Scale Structure in High Reynolds Number ($R_\lambda \sim$ 1000) Turbulent Shear Flow," *Phys. Fluids*, Vol. 12, pp. 2976-2989.

Yu D. and Girimaji S. S., 2005, "DNS of Homogeneous Shear Turbulent Revisited with the Lattice Boltzmann Method," *J. Turbulence.*, Vol. 6, pp. 1-17.

FIGURES

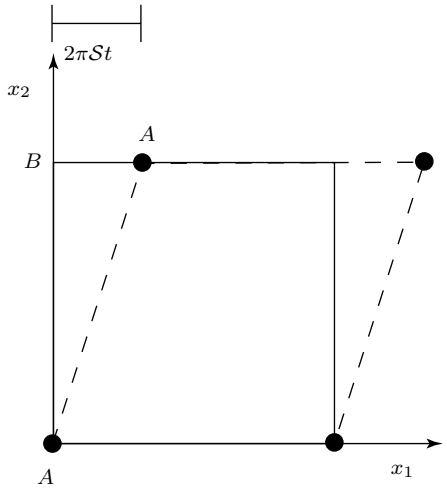

Figure 1: Schematic of the shear periodic boundary conditions in two dimensions. Mean shear of magnitude $\mathcal{S}$ lies in the vertical direction. Solid lines indicate orthogonal frame; dashed lines indicate deforming frame in which boundary conditions are periodic. Black dots are periodic points.

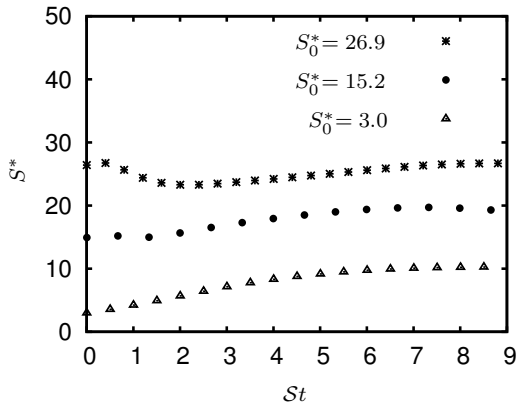

Figure 2: Time evolution of the shear parameter, S^*, for indicated initial values of S_0^* and $R_\lambda \sim 26$.

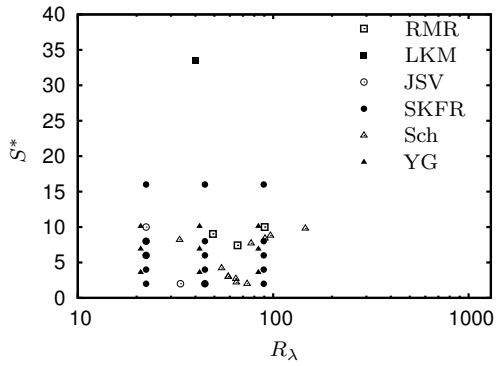

Figure 3: Initial values of S_0^* and R_λ in previous DNS studies. RMR is Rogers *et al* (1986); LKM is Lee *et al*, (1990); JSV is Jacobitz *et al* (1997); SKFR is Shih *et al* (2000); Sch is Schumacher (2004); and YG is Yu and Girimaji (2005).

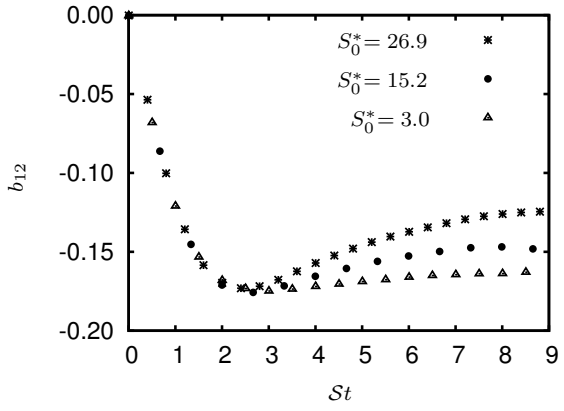

Figure 4: Time evolution of the Reynolds stress for the indicated initial values of S_0^* and $R_\lambda \sim 26$.

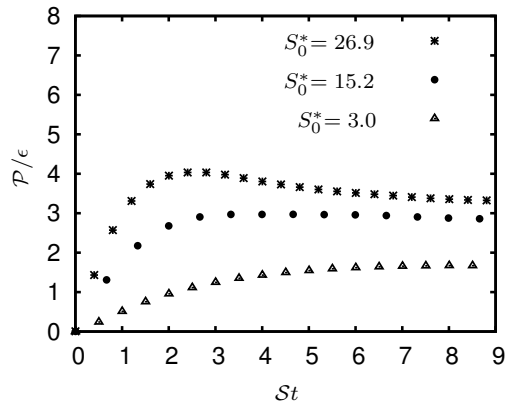

Figure 5: Time evolution of $\mathcal{P}/\epsilon$ for the indicated initial values of S_0^* and $R_\lambda \sim 26$.

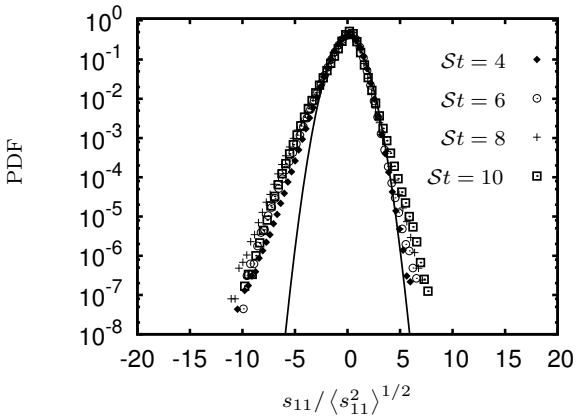

Figure 6: Time evolution of the PDF of s_{11} at the indicated values of $\mathcal{S}t$ and for $S_0^* = 26.9$ and $R_\lambda \sim 26$.

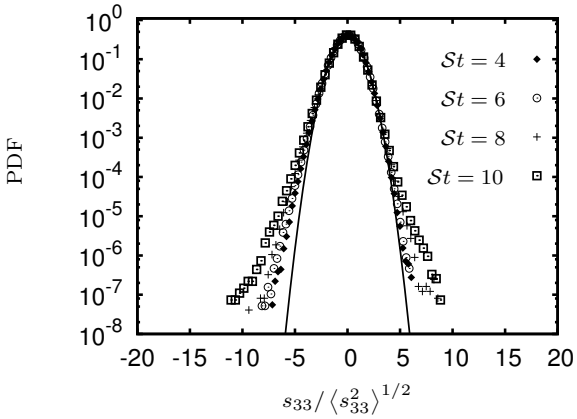

Figure 7: Time evolution of the PDF of s_{33} at the indicated values of $\mathcal{S}t$ and for $S_0^* = 26.9$ and $R_\lambda \sim 26$.

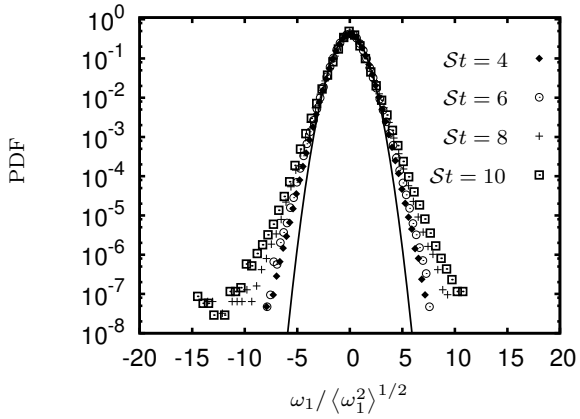

Figure 8: Time evolution of the PDF of ω_1 at the indicated values of $\mathcal{S}t$ and for $S_0^* = 26.9$ and $R_\lambda \sim 26$.

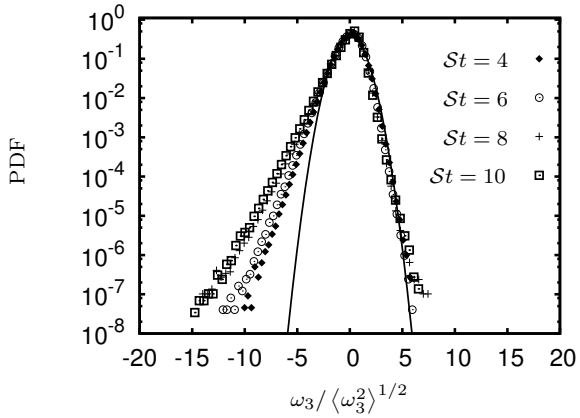

Figure 9: Time evolution of the PDF of ω_3 at the indicated values of $\mathcal{S}t$ and for $S_0^* = 26.9$ and $R_\lambda \sim 26$.

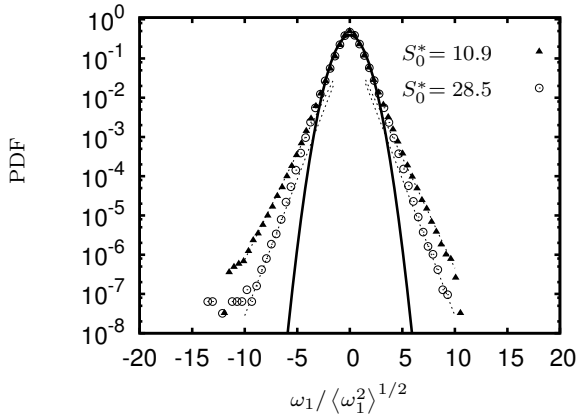

Figure 10: Effect of the initial shear parameter, S_0^*, on the PDF of ω_1 for fixed $R_\lambda \sim 55$.

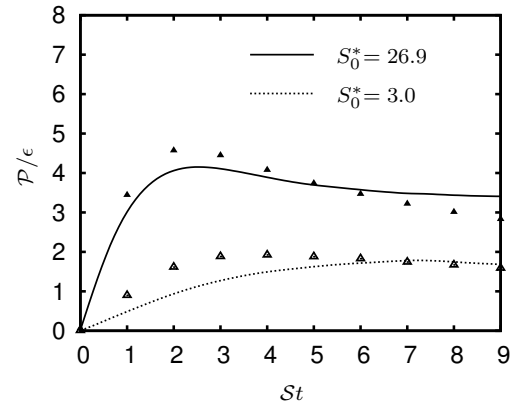

Figure 11: Comparison of the time evolution of P/ϵ from VRDT (markers) and DNS (lines) for the two indicated initial values of S_0^* and $R_\lambda \sim 26$.

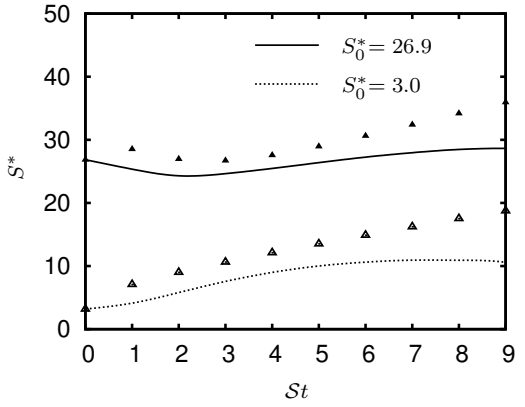

Figure 12: Comparison of the time evolution of S^* from VRDT (markers) and DNS (lines) for the two indicated initial values of S_0^* and $R_\lambda \sim 26$.

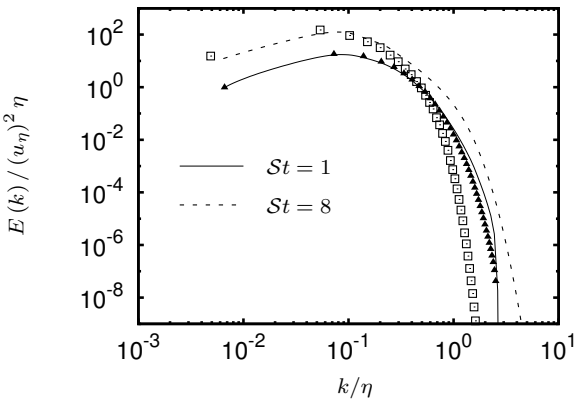

Figure 13: Comparison of the time evolution of the energy spectra predicted by RDT (markers) and DNS (lines) at the two indicated times for $S_0^* = 26.9$ and $R_\lambda \sim 26$.